Applied Numerical Mathematics 141 (2019) 144–157

Contents lists available at ScienceDirect

Applied Numerical Mathematics

www.elsevier.com/locate/apnum

Long wave dynamics for a liquid CO_2 lake in the deep ocean

Krister J. Trandal, Henrik Kalisch *

Department of Mathematics, University of Bergen, 5020 Bergen, Norway

ARTICLE INFO

Article history:
Available online 28 January 2019

Keywords:
Interfacial waves
Kelvin–Helmholtz instability
Liquid carbon-dioxide
Deep ocean experiments

ABSTRACT

A long-wave model for the evolution of long waves at the interface of a deep and a shallow fluid is put forward. The model allows for a uniform stream in one of the layers, and the existence of interfacial capillarity. The model can be used to study the dynamics of the interface between liquid CO_2 and seawater in the deep ocean, including the evolution of the hydrate layer.

If restricted to unidirectional waves the model has the form of a Benjamin-type equation found by Benjamin [2]. Steady periodic solutions of the Benjamin equation are found using a numerical bifurcation code based on a pseudo-spectral projection. The bifurcation patterns are complex, with some branches featuring turning points and secondary bifurcations.

1. Introduction

In this paper, we study the motion of a free interface between two inviscid fluid layers in the presence of interfacial tension in the case when one of the fluids features a uniform flow parallel to the interface. The motivation for this problem comes from recent suggestions that it might be possible to capture CO_2 from combustion processes, and sequester the CO_2 in the form of an underwater lake in the deep ocean [10,18]. Given predominant oceanic temperatures, CO_2 condenses to the liquid phase at a pressure of about 4100 kPa, corresponding to a depth of about 400 m [5,15]. CO_2 in liquid form is still slightly compressible, and if it is located at depths larger than about 3000 m in the ocean, its density will be greater than that of seawater, and there is a possibility for stable storage in a large underwater depression (see Fig. 1).

On the other hand, since the density differential between CO_2 and seawater is not great even at very large depths, the stability of the interface between the two liquids is a critical issue for secure storage. Otherwise, large-scale perturbations of the interface might lead to bubbling up of CO_2 and over decades to eventual depletion of the underwater storage site. As it turns out, CO_2 combines with H_2O to form an icelike solid known as hydrate, and the hydrate layer at the interface actually contributes to the stability of the interface. While it is sometimes modeled by including capillarity at the interface, recent experiments have shown that this approach to modeling the hydrate layer may not be appropriate as the hydrate layer is often broken into several pieces by strong wave motion. Nevertheless, significant efforts have been expended to evaluate the interfacial tension due to the hydrate layer. For example [21] reports on laboratory experiments under high pressure while [5] reports on wavetank experiments at 4000 m depth designed to uncover the nature of the hydrate layer at large depth, and [11] investigates the strength of the capillarity in the deep-sea experiments.

* Corresponding author.
E-mail addresses: krister.trandal@gmail.com (K.J. Trandal), henrik.kalisch@uib.no (H. Kalisch).

https://doi.org/10.1016/j.apnum.2019.01.012
0168-9274/

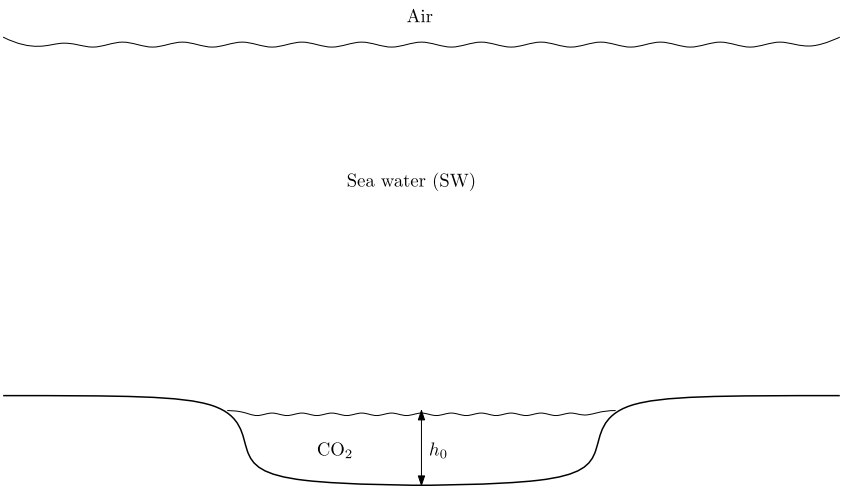

Fig. 1. A lake of liquid CO_2 in a depression on the sea floor.

In the current work, we put forward a simple model equation which describes the wave motion at an interface between a shallow and a deep fluid. For the sake of being explicit, it is assumed that the upper layer is infinite, and features a background current.

We study the case of interfacial waves which are long when compared to the depth of the lower fluid. In this case, the problem is readily reduced to relatively simple model equations of Boussinesq type. The equations feature a non-local term which arises due to the large depth of the upper fluid. This dispersive term is in competition with the third-order term which originates from the inclusion of capillarity. In addition, there is a term which is due to the nonzero background stream of the upper fluid which is motivated by the modeling of bottom currents in the ocean.

Since the uniform stream in the upper layer drives waves predominantly in a single direction, it is natural to restrict the system to a unidirectional model. If this is done, a single model equation appears. The equation has the form

$$\eta_t + \eta_x + \frac{3}{2}\eta\eta_x - \beta\,\mathcal{H}\eta_{xx} - \gamma\,\eta_{xxx} = 0,$$

for certain values of β and γ which will be obtained in the body of the paper. As it turns out, this equation is similar to an equation found by Benjamin [2,12], but the presence of the uniform flow in the upper fluid features prominently in one of the coefficients. In order to solve this equation, we resort to a recently published open-source Python solver called `SpecTraVVave` [14]. In particular, we analyze the bifurcation diagram for steady solutions of the equation, and show that it features a number of interesting features such as turning points, secondary bifurcations and interconnected branches.

2. Problem formulation

The object of study in this work is wave motion in a two-fluid system, separated by a sharp density interface located in the undisturbed state at $z = 0$ in a two-dimensional Cartesian xz-coordinate system. The fluids are assumed to have constant but possibly different densities, and the flow to be inviscid and irrotational in each layer. Furthermore, the velocity of the basic flow[1] is assumed to be zero in the lower layer, while horizontal and uniform in the upper layer. See Fig. 2 for a depiction along with a further description of the variables involved.

From the incompressible continuity equation and the assumption of irrotational flow, one finds that the velocity potential for each layer must satisfy Laplace's equation. That is,

$$\begin{aligned} \triangle\psi &= 0 \quad \text{in} \quad \eta < z < \infty, \\ \triangle\phi &= 0 \quad \text{in} \quad -h_0 < z < \eta, \end{aligned}$$

together with the requirements that

$$\psi_z \to 0 \quad \text{if} \quad z \to \infty, \tag{1}$$

$$\phi_z = 0 \quad \text{at} \quad z = -h_0, \tag{2}$$

[1] We adopt the terminology from [8]. The term *basic flow* refers to the background flow that is present independent of interface deflection. The term *disturbed flow* then describes the flow that arise due to interface deflection. These two flows are superposed to give a total flow field. The potentials ψ and ϕ that appear represent the unknown disturbed flow field.

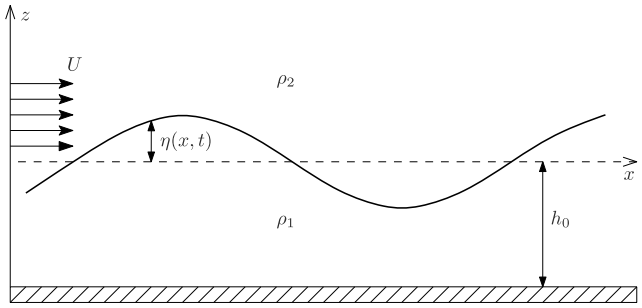

Fig. 2. A schematic of the two-fluid interface problem. In the upper layer, with density ρ_2, there is an imposed horizontal shear velocity U. The upper layer is assumed to be infinitely deep while the lower layer, with density ρ_1, has finite, constant depth h_0. The function $z = \eta(x,t)$ represents the interface deflection at position x and time t. For visual clarity the wave amplitude is greatly exaggerated.

for the problem at hand. Condition (1) states that the flow field should remain uniform far from the interface, while eq. (2) is the no-penetration boundary condition at the rigid bed. We assume that the variation in the transverse y-direction is negligible.

At the fluid interface, the following kinematic and dynamic boundary conditions are imposed:

$$\left.\begin{array}{lrcl} \text{(a)} & \eta_t + (\psi_x + U)\eta_x &=& \psi_z, \\ \text{(b)} & \eta_t + \phi_x\eta_x &=& \phi_z, \\ \text{(c)} & p_1 - p_2 &=& -\tau\eta_{xx}, \end{array}\right\} \text{ at } z = \eta, \tag{3}$$

where p_1 and p_2 are the pressures in the fluid layers, measured close to the interface. The variable τ is the interfacial tension parameter. The dynamic boundary condition (3c) may be rewritten with the help of a Bernoulli equation as

$$\rho_1\left(g\eta + \phi_t + \tfrac{1}{2}\phi_x^2 + \tfrac{1}{2}\phi_z^2\right) - \rho_2\left(g\eta + \psi_t + \tfrac{1}{2}\psi_x^2 + U\psi_x + \tfrac{1}{2}\psi_z^2\right) = \tau\,\eta_{xx}. \tag{4}$$

The existence of the interfacial hydrate layer is one of the defining properties of the configuration of a lower layer of compressed liquid CO_2 and an upper layer of seawater. In a number of works, the existence of the hydrate layer has been described mathematically by altering the value of interfacial tension. It will be shown in the next section how this parameter can be found approximately using deep-water experiments with a wave flume containing liquid CO_2 and a thruster above the flume which creates a background current in the ambient seawater.

3. Dispersion relation

To find the linear dispersion relation, we solve the Laplace problems in the upper and lower domains with the boundary conditions (1) and (2). In the derivation of the dispersion relation, we take a slightly more general view than above, subject use the interface conditions (3a), (3b), (3c), with a background stream U_2 instead of U in the upper layer, and a background stream U_1 in the lower layer. We apply the method of normal modes [16, pp. 469–470] and assume a sinusoidal waveform in each layer when the interface is disturbed:

$$\phi(x,z,t) = A_1(z)e^{ik(x-ct)}, \quad \psi(x,z,t) = A_2(z)e^{ik(x-ct)}.$$

Substitution into the Laplace equations and dividing out the exponential factor results in the two ODEs

$$\frac{d^2A_1}{dz^2} - k^2A_1 = 0, \quad \frac{d^2A_2}{dz^2} - k^2A_2 = 0,$$

whose general solutions are found to be

$$A_1(z) = a_1e^{|k|z} + b_1e^{-|k|z}, \quad A_2(z) = a_2e^{|k|z} + b_2e^{-|k|z}.$$

With the conditions given in (1) and (2), we require that $a_2 = 0$ and $b_1 = a_1e^{-2|k|h_0}$. Now apply the linearized kinematic conditions (3a) and (3b) to determine a_1 and b_2. We assume an interfacial shape of the form $\eta(x,t) = \eta_0e^{ik(x-ct)}$, and thereby obtain

$$\begin{aligned} -U_1ik\eta_0e^{ik(x-ct)} + a_1|k|(e^{|k|z} - e^{-|k|z-2|k|h_0})e^{ik(x-ct)} &= -\eta_0ikce^{ik(x-ct)} \\ &= -U_2ik\eta_0e^{ik(x-ct)} - b_2|k|e^{ik(x-ct)-|k|z}, \end{aligned}$$

or

$$-U_1 ik\eta_0 + a_1|k|(e^{|k|z} - e^{-|k|z-2|k|h_0}) = -ikc\eta_0 = -U_2 ik\eta_0 - b_2|k|e^{-|k|z},$$

which, at $z = 0$, simplifies to

$$-U_1 ik\eta_0 + a_1|k|(1 - e^{-2|k|h_0}) = -ikc\eta_0 = -U_2 ik\eta_0 - b_2|k|.$$

Hence

$$a_1 = i\,\eta_0 \frac{U_1 - c}{1 - e^{-2kh_0}}\mathrm{sgn}(k), \quad b_2 = i\,\eta_0(c - U_2)\mathrm{sgn}(k).$$

Now substitute the expressions for ϕ, ψ and η into the linearized dynamic condition (3c) to obtain, after some algebraic manipulations, a quadratic equation in the wave speed c:

$$\{\rho_1 k\coth(kh_0) + \rho_2|k|\}c^2 - \{2\rho_1 kU_1\coth(kh_0) + 2\rho_2 U_2|k|\}c + \left\{\rho_1 U_1^2 k\coth(kh_0) + \rho_2 U_2^2|k| + (\rho_2 - \rho_1)g - \tau k^2\right\} = 0. \tag{5}$$

Solving this equation for c, we extract the following linear dispersion relation:

$$c(k) = \frac{\rho_1 U_1 k\theta + \rho_2 U_2|k|}{\rho_1 k\theta + \rho_2|k|} \pm \frac{1}{\rho_1 k\theta + \rho_2|k|} \cdot \left\{\tau k^2(\rho_1 k\theta + \rho_2|k|) - \rho_1\rho_2(U_1 - U_2)^2 k|k|\theta + (\rho_1 - \rho_2)(\rho_1 k\theta + \rho_2|k|)g\right\}^{1/2}, \tag{6}$$

where $\theta = \coth(kh_0)$.

3.1. Long-wave and short-wave approximations

One can obtain a long-wave or shallow water approximation of the above dispersion relation (5). In this case, k will be small,[2] and from the expansion of the hyperbolic function in its argument, we find that

$$(kh_0)\coth(kh_0) = 1 + \frac{(kh_0)^2}{3} + \mathcal{O}\left((kh_0)^3\right) \approx 1, \tag{7}$$

where the approximate equality holds for small kh_0. So the long-wave approximation to the dispersion relation (5) is

$$\{\rho_1 + \rho_2 h_0|k|\}c^2 - \{2\rho_1 U_1 + 2\rho_2 h_0 U_2|k|\}c + \left\{\rho_1 U_1^2 + \rho_2 h_0 U_2^2|k| + (\rho_2 - \rho_1)h_0 g - h_0\tau k^2\right\} = 0. \tag{8}$$

For the opposite scenario, the short-wave or deep water approximation, the wave number k is large. In a similar argument to that given in (7), the hyperbolic function $\coth(kh_0)$ may be replaced by unity to give

$$\{\rho_1 k + \rho_2|k|\}c^2 - \{2\rho_1 U_1 k + 2\rho_2 U_2|k|\}c + \left\{\rho_1 U_1^2 k + \rho_2 U_2^2|k| + (\rho_2 - \rho_1)g - \tau k^2\right\} = 0, \tag{9}$$

which is the short-wave approximation to (5). The corresponding wave speed solutions for the two cases can be extracted from (6) by applying the appropriate approximations just described.

3.2. Evaluation of the surface tension parameter

A quantification of the surface tension parameter τ will now be given using deep ocean experiments with liquid CO_2 conducted at about 4000 m depth. In these experiments, which were described in detail in [5], a wave flume was lowered to the ocean bottom at about 4000 m depth and filled with liquid CO_2. A thruster just above the wave flume was run at various speeds, simulating the occurrence of ocean shear currents of varying strength. Alternatively, waves were created with a wavemaker at one end of the tank. The experiments were investigated at length in [11]. In particular the authors aimed at obtaining estimates for the surface tension parameter using the results from runs with the wavemaker, but the analysis was somewhat inconclusive. Here, we use the response of the CO_2-seawater interface to different thruster settings in order to estimate the surface tension parameter.

The thruster experiments described in [5] and [11] can be summarized as follows. If the current in the seawater had a small enough velocity, then the flow appeared laminar, while high thruster settings led to a completely turbulent flow. The critical shear velocity was found to be $U_c = 17.6$ cm/s. It is reasonable to assume that the turbulence developed from small disturbances via Kelvin–Helmholtz instabilities at the interface and the hydrate layer. Thus, using the critical velocity as a

[2] In shallow water, h_0 is small. Throughout this study, we are assuming that the undisturbed lower layer depth h_0 is fixed.

given parameter, one may inspect the dispersion relation (6), and find the corresponding value of the τ which makes the velocity $U_c = 17.6$ cm/s critical.

To get an initial approximation, we assume that instabilities are mainly due to short waves. Moreover, we assume that the dominant instability can be captured using a two-dimensional analysis. This assumption depends on the particular situation, but will certainly be valid if the transverse variation in the background stream is weak, such as in the wave flume experiment under study.

From (9), if the lower layer is quiescent, and the background flow in the upper layer is given by $U_2 = U$, the short wave approximation of the dispersion relation is

$$c = \frac{\rho_2 U}{\rho_1+\rho_2} \pm \frac{1}{(\rho_1+\rho_2)k}\left\{(\rho_1+\rho_2)\tau k^3 - \rho_1\rho_2 U^2 k^2 + (\rho_1^2-\rho_2^2)gk\right\}^{\frac{1}{2}} \tag{10}$$

Recalling that the interface Fourier modes are assumed to be of the form $\eta = \eta_0 e^{i(kx-\omega t)} = \eta_0 e^{ik(x-ct)}$, it is clear that imaginary values of c yield solutions with exponential growth. To avoid this, we require that the discriminant from the approximate expression (10) satisfy

$$D_{\text{approx}}(k) := (\rho_1+\rho_2)\tau k^2 - \rho_1\rho_2 U^2 k + (\rho_1^2-\rho_2^2)g > 0. \tag{11}$$

Differentiating $D_{\text{approx}}(k)$ with respect to k, we find that (11) holds true if

$$\tau = \frac{\rho_1^2\rho_2^2 U^4}{4(\rho_1+\rho_2)(\rho_1^2-\rho_2^2)g}. \tag{12}$$

Using the critical velocity $U = U_c$, in addition to the values from Table 2, we find from eq. (12) that $\tau \approx 0.21$. This approximate value for τ may be used further in the full dispersion relation to obtain a more accurate approximation to the interfacial surface tension. This time, instead of differentiating the discriminant in the dispersion relation, denoted by $D(k)$, we wrote a Python program to find a value for τ that makes $\min_k D(k)$ positive and close to zero. Our finding is that

$$\tau \approx 0.22003 \text{ N/m}.$$

Thus this value should be used if the hydrate layer at the interface of seawater and liquid CO_2 is to be modeled by interfacial capillarity in the conditions of the experiments described in [5] and [11].

4. Derivation of the model equations

We now desire to derive a model system describing long-crested waves on fairly shallow water, and further restrict our attention to waves propagating in one direction on the interface between two immiscible fluids. The subsequent derivation of the nonlinear equations is similar to the treatment given in [12] and [20, pp. 464–466].

4.1. Nondimensionalization

In order to make the assumptions on the geometry of the domain and the waves visible, and be able to deduce the relative order and importance of terms, we perform the following scaling on the variables:

$$z' = \lambda Z \quad \text{in} \quad \eta' < z' < \infty,$$
$$z' = h_0 z \quad \text{in} \quad -h_0 < z' < \eta',$$

where original variables appear primed. Notice the different scaling used in the two fluid layers. Furthermore, we let

$$x' = \lambda x, \quad t' = \frac{\lambda}{c_0 v_0} t, \tag{13}$$

and

$$\eta' = a\eta, \quad \phi' = \frac{ag\lambda v_0}{c_0}\phi, \quad \psi' = \frac{ag\lambda v_0}{c_0}\psi, \tag{14}$$

where $c_0 = \sqrt{gh_0}$ is the limiting shallow water wave speed, and $v_0^2 = 1 - \frac{\rho_2}{\rho_1}$. We also introduce the parameters

$$\varepsilon = \frac{h_0}{\lambda}, \quad \sigma = \frac{a}{h_0}, \quad \mu = \frac{\tau}{(\rho_1-\rho_2)g\lambda^2},$$

where ε, σ, μ are assumed to be small and of the same order. The parameter μ is similar to that of a reciprocal Bond number, and displays the relative importance of capillary effects versus gravity effects.

In normalized variables, the two kinematic boundary conditions (3a), (3b) are converted to

$$\eta_t + \left(\sigma\psi_x + \frac{U}{c_0 v_0}\right)\eta_x = \frac{1}{\varepsilon}\psi_Z, \tag{15}$$

$$\eta_t + \sigma\phi_x\eta_x = \frac{1}{\varepsilon^2}\phi_z. \tag{16}$$

The dynamic condition (4), after collecting terms and dividing out common factors, becomes

$$\eta + \phi_t + \frac{1}{2}\sigma\phi_x^2 + \frac{1}{2}\frac{\sigma}{\varepsilon^2}\phi_z^2 - \frac{\rho_2}{\rho_1}\left\{\psi_t + \frac{1}{2}\sigma\psi_x^2 + \frac{1}{2}\sigma\psi_Z^2 + \frac{U}{c_0 v_0}\psi_x\right\} - \mu\eta_{xx} = 0. \tag{17}$$

4.2. Nonlinear system of equations

Subtracting eq. (16) from eq. (15) and rearranging, we get

$$\psi_Z = \frac{1}{\varepsilon}\phi_z + \varepsilon\frac{U}{c_0 v_0}\eta_x + \mathcal{O}(\varepsilon\sigma), \quad Z = \varepsilon\sigma\eta. \tag{18}$$

In conjunction with the developments given in [20, pp. 460–466], we now desire to write a formal expansion for ϕ in powers of the vertical coordinate z, in our case about $z = -1$:

$$\phi = \sum_{n=0}^{\infty}(z+1)^n f_n(x,t).$$

Substitution into the normalized Laplace equation $\varepsilon^2\phi_{xx} + \phi_{zz} = 0$ and the boundary condition $\phi_z(z=-1) = 0$ at the bottom of the lower layer give[3]

$$\phi = \sum_{n=0}^{\infty}(-1)^n\frac{\varepsilon^{2n}}{(2n)!}(z+1)^{2n}\frac{\partial^{2n}}{\partial x^{2n}}f(x,t) = f - \frac{1}{2}\varepsilon^2(z+1)^2 f_{xx} + \mathcal{O}(\varepsilon^4),$$

where f_0 is now labeled f. This expression for ϕ gives

$$\phi_z = -\varepsilon^2(z+1)f_{xx} + \mathcal{O}(\varepsilon^4). \tag{19}$$

Hence, from (18) we get

$$\psi_Z = -\varepsilon(1+\sigma\eta)f_{xx} + \varepsilon\frac{U}{c_0 v_0}\eta_x + \mathcal{O}(\varepsilon^2, \varepsilon\sigma), \quad Z = \varepsilon\sigma\eta. \tag{20}$$

We are then left with the Laplace equation for ψ. With the condition (20), the following elliptic problem appears

$$\begin{cases} \triangle\psi = 0, \quad Z > \varepsilon\sigma\eta, \\ \psi_Z = -\varepsilon(1+\sigma\eta)f_{xx} + \varepsilon\frac{U}{c_0 v_0}\eta_x + \mathcal{O}(\varepsilon^2, \varepsilon\sigma), \quad Z = \varepsilon\sigma\eta. \end{cases} \tag{21}$$

Expanding the boundary condition function ψ_Z in a Taylor series about $Z = 0$ allows the problem (21) to be shifted to the more tractable half-plane problem

$$\begin{cases} \triangle\psi = 0, \quad Z > 0, \\ \psi_Z = -\varepsilon f_{xx} + \varepsilon\frac{U}{c_0 v_0}\eta_x + \mathcal{O}(\varepsilon^2, \varepsilon\sigma), \quad Z = 0. \end{cases} \tag{22}$$

The solution of this upper half-plane Neumann problem is given by

$$\psi = -\varepsilon\mathcal{H}\left(\partial_x^{-1}P(Z)\left[f_{xx} - \frac{U}{c_0 v_0}\eta_x\right]\right) + \mathcal{O}(\varepsilon^2, \varepsilon\sigma),$$

where $\mathcal{H}$ is the Hilbert transform, which is defined by

$$\mathcal{H}[f](x) = \text{p.v.}\frac{1}{\pi}\int_{-\infty}^{\infty}\frac{f(x-y)}{y}\,dy,$$

[3] All the terms of odd power vanish by virtue of the bottom layer boundary condition.

with p.v. denoting the Cauchy principal value. Throughout this paper, the Hilbert transform is taken in the spatial variable $x \in \mathbb{R}$. The notation $P(\cdot)$ signifies a Poisson integral operator for the upper half-plane. Furthermore, we obtain

$$\psi(Z=0) = -\varepsilon\mathcal{H}\left(f_x - \frac{U}{c_0 v_0}\eta\right) + \mathcal{O}(\varepsilon^2, \varepsilon\sigma),$$

and

$$\psi_x(Z=0) = -\varepsilon\mathcal{H}\left(f_{xx} - \frac{U}{c_0 v_0}\eta_x\right) + \mathcal{O}(\varepsilon^2, \varepsilon\sigma).$$

To briefly summarize, we have that, at the interface

$$\phi_t = f_t + \mathcal{O}(\varepsilon^2), \quad \phi_x = f_x + \mathcal{O}(\varepsilon^2), \quad \phi_z = -\varepsilon^2(1+\sigma\eta)f_{xx},$$
$$\psi_t = -\varepsilon\mathcal{H}\left(f_{xt} - \frac{U}{c_0 v_0}\eta_t\right) + \mathcal{O}(\varepsilon^2, \varepsilon\sigma), \psi_x = -\varepsilon\mathcal{H}\left(f_{xx} - \frac{U}{c_0 v_0}\eta_x\right) + \mathcal{O}(\varepsilon^2, \varepsilon\sigma), \quad \psi_Z = \mathcal{O}(\varepsilon).$$

Substitution of these expressions into the normalized dynamic condition (17) gives

$$\eta + f_t + \frac{1}{2}\sigma f_x^2 + \varepsilon\frac{\rho_2}{\rho_1}\mathcal{H}\left(f_{xt} - \frac{U}{c_0 v_0}\eta_t + \frac{U}{c_0 v_0}f_{xx} - \frac{U^2}{c_0^2 v_0^2}\eta_x\right) - \mu\eta_{xx} = \mathcal{O}(\varepsilon^2, \varepsilon\sigma, \sigma^2, \ldots).$$

Differentiating with respect to x and writing $w = f_x$ yields

$$\eta_x + w_t + \sigma w w_x + \varepsilon\frac{\rho_2}{\rho_1}\mathcal{H}\left(w_{xt} - \frac{U}{c_0 v_0}\eta_{xt} + \frac{U}{c_0 v_0}w_{xx} - \frac{U^2}{c_0^2 v_0^2}\eta_{xx}\right) - \mu\eta_{xxx} = \mathcal{O}(\varepsilon^2, \varepsilon\sigma, \sigma^2, \ldots). \tag{23}$$

From this, it is evident that $\eta_x + w_t = \mathcal{O}(\varepsilon, \mu, \sigma)$. Assuming that differentiation and the application of $\mathcal{H}$ does not alter this order relation (cf. [12, p. 172]), we have

$$\mathcal{H}w_{xt} = -\mathcal{H}\eta_{xx} + \mathcal{O}(\varepsilon, \mu, \sigma). \tag{24}$$

Also, from the kinematic condition (16),

$$\eta_t + \sigma(w + \mathcal{O}(\varepsilon^2))\eta_x + (1+\sigma\eta)w_x + \mathcal{O}(\varepsilon^2) = 0.$$

This gives $\eta_t + w_x = \mathcal{O}(\varepsilon^2, \sigma)$ and, under the same assumptions leading to (24),

$$\mathcal{H}\eta_{xt} = -\mathcal{H}w_{xx} + \mathcal{O}(\varepsilon^2, \sigma). \tag{25}$$

Substitution of (24) and (25) into (23) results in

$$\eta_x + w_t + \sigma w w_x + \varepsilon\frac{\rho_2}{\rho_1}\mathcal{H}\left(2\frac{U}{c_0 v_0}w_{xx} - \eta_{xx} - \frac{U^2}{c_0^2 v_0^2}\eta_{xx}\right) - \mu\eta_{xxx} = \mathcal{O}(\varepsilon^2, \varepsilon\sigma, \sigma^2, \ldots)$$

Neglecting terms of quadratic and higher order in ε, σ and μ, we obtain the system

$$\begin{cases} \eta_x + w_t + \sigma w w_x + \varepsilon\frac{\rho_2}{\rho_1}\left(\frac{2U}{c_0 v_0}\mathcal{H}w_{xx} - \mathcal{H}\eta_{xx} - \frac{U^2}{c_0^2 v_0^2}\mathcal{H}\eta_{xx}\right) - \mu\eta_{xxx} = 0, \\ \eta_t + w_x + \sigma(\eta w)_x = 0. \end{cases} \tag{26}$$

Changing back to dimensional variables, the model system (26) becomes

$$\begin{cases} g v_0^2\eta_x + w_t + w w_x + \frac{\rho_2}{\rho_1}\left(2U h_0\mathcal{H}w_{xx} - c_0^2 v_0^2\mathcal{H}\eta_{xx} - U^2\mathcal{H}\eta_{xx}\right) - \frac{\tau}{\rho_1}\eta_{xxx} = 0, \\ \eta_t + h_0 w_x + (\eta w)_x = 0. \end{cases} \tag{27}$$

It can be seen that the dispersion relation of the linearized system is the same as the expression (8) obtained for the linearized full problem.

4.3. Unidirectional wave propagation

As already mentioned, our intention is to derive a simple model equation for waves propagating in a single direction, so let us restrict our attention to waves propagating to the right. The nondimensional system (26) will serve as the outset for our development. To find solutions to first order in ε, σ and μ we propose the ansatz (cf. [12, p. 173])

$$w = \eta + \varepsilon A + \sigma B + \mu C$$

where A, B and C are functions of η and its derivatives. Substituting this expression into the nondimensional system (26) and disregarding higher order terms, we get

$$\begin{cases} \eta_t + \eta_x + \varepsilon \left[A_t - \frac{\rho_2}{\rho_1} \left(\frac{U}{c_0 v_0} - 1 \right)^2 \mathcal{H}\eta_{xx} \right] + \sigma \left(B_t + \eta\eta_x \right) + \mu \left(C_t - \eta_{xxx} \right) = 0, \\ \eta_t + \eta_x + \varepsilon A_x + \sigma \left(B_x + 2\eta\eta_x \right) + \mu C_x = 0. \end{cases} \tag{28}$$

Because $A = A(\eta, \eta_t, \eta_x \ldots)$, we may replace A_t by $-A_x$ to quadratic order in ε, and similarly for B and C. Doing so, the system (28) becomes

$$\begin{cases} \eta_t + \eta_x + \varepsilon \left[-A_x - \frac{\rho_2}{\rho_1} \left(\frac{U}{c_0 v_0} - 1 \right)^2 \mathcal{H}\eta_{xx} \right] + \sigma \left(-B_x + \eta\eta_x \right) + \mu \left(-C_x - \eta_{xxx} \right) = 0, \\ \eta_t + \eta_x + \varepsilon A_x + \sigma \left(B_x + 2\eta\eta_x \right) + \mu C_x = 0, \end{cases} \tag{29}$$

after higher order terms have been neglected. For consistency between the equations in (29), we require

$$\begin{aligned} A_x &= -A_x - \frac{\rho_2}{\rho_1} \left(\frac{U}{c_0 v_0} - 1 \right)^2 \mathcal{H}\eta_{xx}, \\ B_x + 2\eta\eta_x &= -B_x + \eta\eta_x, \\ C_x &= -C_x - \eta_{xxx}, \end{aligned}$$

which after rearrangement and integration gives

$$A = -\frac{1}{2} \frac{\rho_2}{\rho_1} \left(\frac{U}{c_0 v_0} - 1 \right)^2 \mathcal{H}\eta_x, \quad B = -\frac{1}{4}\eta^2, \quad C = -\frac{1}{2}\eta_{xx}.$$

Consequently,

$$w = \eta - \varepsilon \frac{1}{2} \frac{\rho_2}{\rho_1} \left(\frac{U}{c_0 v_0} - 1 \right)^2 \mathcal{H}\eta_x - \frac{1}{4}\sigma\eta^2 - \frac{1}{2}\mu\eta_{xx}.$$

Substituting this expression for w into the second equation in (26) and dropping quadratic terms, we obtain the model equation

$$\eta_t + \eta_x + \sigma \frac{3}{2}\eta\eta_x - \varepsilon \frac{1}{2} \frac{\rho_2}{\rho_1} \left(\frac{U}{c_0 v_0} - 1 \right)^2 \mathcal{H}\eta_{xx} - \mu \frac{1}{2}\eta_{xxx} = 0. \tag{30}$$

In equation (30), the quantities ε, σ and μ are unknown (they contain the unknown wave parameters a and λ). To circumvent this issue for the purpose of studying the equation numerically, we will subsequently return to dimensional variables and from there apply a second normalization. The model equation (30) in dimensional variables takes the form

$$\frac{1}{c_0 v_0}\eta_t + \eta_x + \frac{1}{h_0}\frac{3}{2}\eta\eta_x - h_0 \frac{1}{2} \frac{\rho_2}{\rho_1} \left(\frac{U}{c_0 v_0} - 1 \right)^2 \mathcal{H}\eta_{xx} - \frac{1}{2} \frac{\tau}{(\rho_1 - \rho_2)g} \eta_{xxx} = 0. \tag{31}$$

We now apply a normalization similar to that given in [4]. As before, original variables appear with a prime.

$$x' = h_0 x, \quad z' = h_0 z, \quad \eta' = h_0 \eta, \quad t' = \frac{h_0}{c_0 v_0} t.$$

Substituting these expressions into (31) and applying the chain rule of differentiation, we finally arrive at the model equation

$$\eta_t + \eta_x + \frac{3}{2}\eta\eta_x - \beta\, \mathcal{H}\eta_{xx} - \gamma\, \eta_{xxx} = 0, \tag{32}$$

where

$$\beta = \frac{1}{2}\frac{\rho_2}{\rho_1}\left(\frac{U}{c_0 v_0} - 1\right)^2, \quad \gamma = \frac{1}{2}\frac{\tau}{(\rho_1 - \rho_2) g h_0^2}. \tag{33}$$

Equation (32) is actually the so-called Benjamin equation which was found in [2], and treated subsequently in [6,7,12–14]. The main difference is the dependence of the coefficient for the nonlocal term on the velocity of the background flow. As it turns out, this dependence has major implications, as it can completely change the nature of the equation, if for example the coefficient vanishes. Note that if γ vanishes, the Benjamin–Ono equation appears. This equation was introduced in [1].

5. Numerical method

In this section, the numerical procedure for approximating traveling wave solutions of eq. (32) is presented. The scheme is a spectral collocation method combined with a numerical continuation procedure for solving the nonlinear algebraic system that arise, and is implemented in a Python-based solver called `SpecTraVVave`. We will here elucidate the main features of the numerical method used in the package, briefly repeating what is presented in [14] to make the current discussion comprehensive. More details on workflow and class descriptions can be found in the source just cited and in the online repository [17].

5.1. Preamble

The package `SpecTraVVave` is written to tackle nonlinear dispersive equations of the general form

$$u_t + [f(u)]_x + \mathcal{L}[u_x] = 0, \tag{34}$$

where $\mathcal{L}$ is a linear, self-adjoint operator, and $f : \mathbb{R} \to \mathbb{R}$ satisfies $f(0) = f'(0) = 0$, in addition to some growth conditions [14, p. 3]. Furthermore, we regard $\mathcal{L}$ as a Fourier multiplier operator. That is,

$$\widehat{\mathcal{L}[u]}(\xi) = \alpha(\xi)\widehat{u}(\xi). \tag{35}$$

Our model equation (32) falls into this category, with

$$f(u) = \frac{3}{4}u^2, \quad \mathcal{L} = 1 - \beta\,\mathcal{H}\,\partial_x - \gamma\,\partial_x^2, \tag{36}$$

where β and γ are as defined in (33). The so-called flux function f and the multiplier function (or *symbol*) α are needed to run the solver. Using that $\widehat{\partial_x u}(\xi) = i\xi\widehat{u}(\xi)$, and $\widehat{\mathcal{H}u}(\xi) = -i\,\mathrm{sgn}(\xi)\widehat{u}(\xi)$ (cf. [14, p. 2]), it is not difficult to derive that

$$\alpha(\xi) = 1 - \beta|\xi| + \gamma\xi^2 \tag{37}$$

for the model equation (32).

5.2. Spectral collocation

The material presented here is analogous to that found in [14] and in [9]. As mentioned in the latter citation, since $\mathcal{L}$ is a Fourier multiplier operator, it is ideal to use a Fourier basis in the spectral method. The cited literature cover models like the Whitham equation, the Benjamin–Ono equation and the Benjamin equation. Our model equation is a type of Benjamin equation [2].

We are interested in computing traveling wave solutions of (34), i.e. solutions in the form

$$u(x,t) = \phi(w), \quad w = x - ct. \tag{38}$$

Substitution into (34) and applying the chain rule gives

$$-c\frac{d\phi}{dw} + \frac{d}{dw}[f(\phi)] + \mathcal{L}\frac{d\phi}{dw} = 0. \tag{39}$$

Integrating once with respect to w yields

$$-c\phi + f(\phi) + \mathcal{L}\phi = B, \tag{40}$$

where B is a constant of integration.

We will further restrict our attention to even periodic solutions of (34). As pointed out in [14, p. 3] this allows us to use a cosine collocation instead of a collocation founded on a more general Fourier basis. Also, because our solutions are even, the method will only need to compute half a solution profile, with the other half constructed by virtue of symmetry.

To be specific regarding the spectral projection, we desire to find approximate solutions in the space

$$\mathcal{S}_N = \mathrm{span}_{\mathbb{R}}\left\{\cos(\kappa_l x) : \kappa_l = \tfrac{2\pi}{L}l,\ 0 < l < N-1\right\} \subset L^2(0,L). \tag{41}$$

The domain is discretized with the collocation points

$$x_n = \frac{L}{2}\frac{2n-1}{2N}, \quad 1 \le n \le N. \tag{42}$$

We then look for a function $\phi_N \in \mathcal{S}_N$ satisfying the equation

$$-c\,\phi_N(x_n) + f(\phi_N)(x_n) + \mathcal{L}^N[\phi_N](x_n) = 0 \tag{43}$$

at each collocation point x_n, yielding a nonlinear algebraic system of N equations in N unknowns,

$$F(\phi_N, c) = 0, \quad F: \mathbb{R}^{N+1} \to \mathbb{R}^N, \tag{44}$$

which can be solved using Newton's method. As ϕ_N is a linear combination of cosines, i.e.

$$\phi_N(x) = \sum_{l=0}^{N-1} \zeta_l \cos(\kappa_l x), \tag{45}$$

its coefficients ζ_l can be computed using the discrete cosine transform (DCT), yielding

$$\zeta_0 = \frac{1}{N}C_0, \quad \zeta_l = \frac{2}{N}C_l, \quad l = 1, ..., N-1, \tag{46}$$

where the DCT $\{C_l\}_{l=0}^{N-1}$ consists of

$$C_l := \sum_{n=0}^{N-1} \phi_N(x_{n+1}) \cos\left(\frac{\pi}{2N}(2n+1)l\right) = \sum_{n=1}^{N} \phi_N(x_n)\cos(\kappa_l x_n), \quad l = 0, ..., N-1.$$

In (43), $\mathcal{L}^N$ is a discrete version of the operator $\mathcal{L}$. Because $\mathcal{L}$ is linear, and because eq. (43) is enforced at the N collocation points, we can evaluate the terms $\mathcal{L}^N[\phi_N](x_n)$ using matrix multiplication. More specifically, we have that

$$\mathcal{L}^N[\phi_N](x_i) = \sum_{j=1}^{N} \mathcal{L}^N(i,j)\phi_N(x_j), \tag{47}$$

where $\mathcal{L}^N(i,j)$ is the matrix defined by

$$\mathcal{L}^N(i,j) = \frac{1}{N}\alpha(0) + \frac{2}{N}\sum_{l=1}^{N-1} \alpha(\kappa_l)\cos(\kappa_l x_i)\cos(\kappa_l x_j). \tag{48}$$

In (48), $\alpha(\cdot)$ is the Fourier multiplier function of the operator $\mathcal{L}$, as defined in eq. (35).

5.3. Numerical continuation and bifurcation branch navigation

`SpecTraVVave` employs a continuation procedure to compute the next solutions of the system (50) and navigate the bifurcation branches. To deal with turning points on the bifurcation curve, both the phase speed and the wave amplitude are assumed to be depending on some parameter, say

$$a = a(\theta), \quad c = c(\theta). \tag{49}$$

The parameter θ is unknown and is to be computed from the extended nonlinear system

$$F\begin{pmatrix} \phi_N(x_1) \\ \phi_N(x_2) \\ \vdots \\ \phi_N(x_N) \\ B \\ \theta \end{pmatrix} = \begin{pmatrix} -c\,\phi_N(x_1) + f(\phi_N)(x_1) + \mathcal{L}^N[\phi_N](x_1) - B \\ -c\,\phi_N(x_2) + f(\phi_N)(x_2) + \mathcal{L}^N[\phi_N](x_2) - B \\ \vdots \\ -c\,\phi_N(x_N) + f(\phi_N)(x_N) + \mathcal{L}^N[\phi_N](x_N) - B \\ \Omega(\phi_N, a, c, B) \\ \phi_N(x_1) - \phi_N(x_N) - a \end{pmatrix} = \begin{pmatrix} 0 \\ 0 \\ \vdots \\ 0 \\ 0 \\ 0 \end{pmatrix} \tag{50}$$

In the system (50), $\Omega(\phi_N, a, c, B)$ is the boundary condition, and the `SpecTraVVave` package offers several choices that can be employed. For our study, we will employ the so-called `Mean()` boundary condition. That is, the condition that the mean of a solution be zero over the region of interest. This choice has roots in the physics of the problem: The mean of a solution profile over, say, a wavelength will have to be zero due to mass conservation (no fluid leaving the lower region, and

Table 1
Physical parameters and their values.

Parameter	Value	Units	Description
g	9.81	m/s^2	acceleration of gravity
h_0	0.11	m	lower layer depth (cf. [11])
ρ_1	1077.0	kg/m^3	lower layer density (cf. [11])
ρ_2	1045.7	kg/m^3	upper layer density (cf. [5])
U_c	0.176	m/s	critical shear velocity (cf. [11])

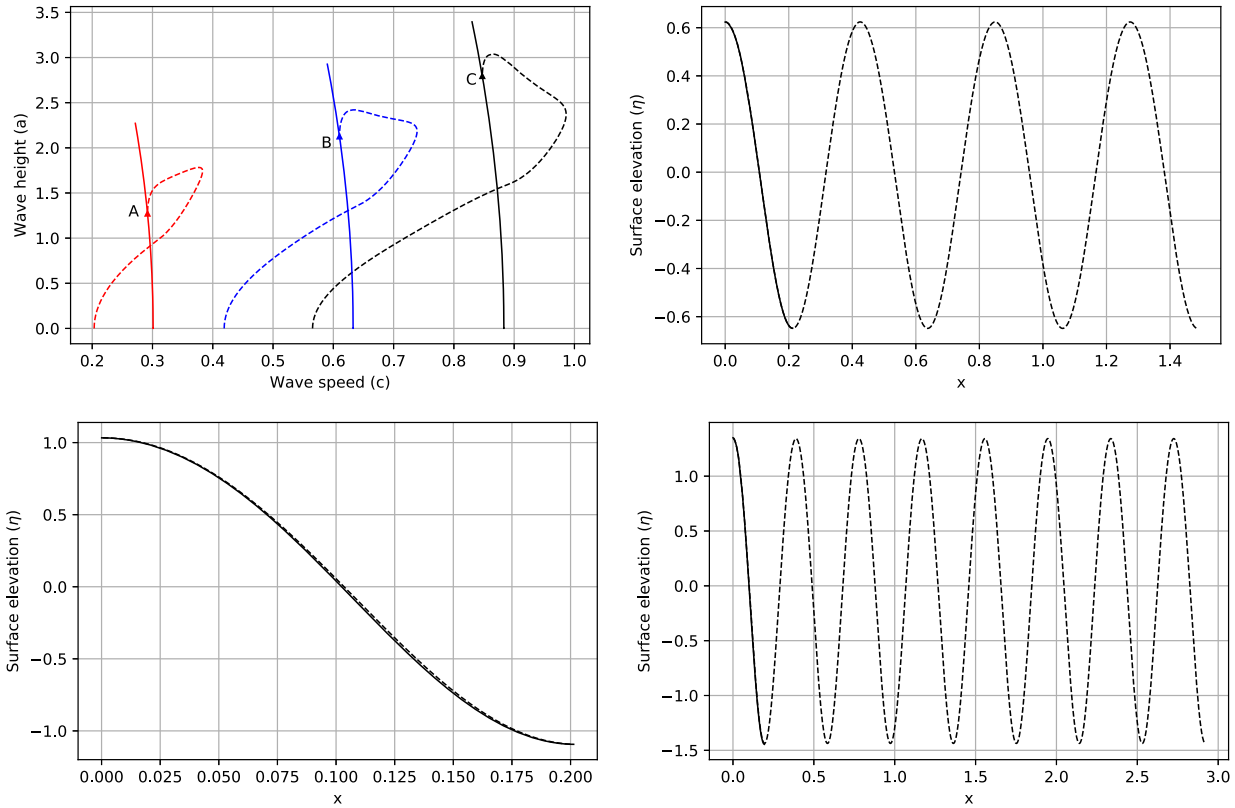

Fig. 3. Multiple connecting bifurcation curves for shear velocity $U = 2c_0v_0$ and parameter values from Table 1, with wave profile at each point of connection. Upper left panel: The branches connect at the points $A = (0.2918, 1.271)$, $B = (0.6102, 2.126)$ and $C = (0.8471, 2.795)$. Upper right panel: Wave profiles at the connection point A for wave numbers $k_3 = 1.85$ (dashed) and $k_3^* = 14.8$ (solid). Lower left panel: Wave profiles at the connection point B, for wave numbers $k_2 = 1.30$ (dashed) and $k_2^* = 15.6$ (solid). This plot is zoomed in, to give an enhanced view of the overlapping profiles. Lower right panel: Wave profiles at the connection point C, for wave numbers $k_1 = 0.95$ (dashed) and $k_1^* = 16.15$ (solid).

interface is initially at rest). The numerical continuation works in a *predictor–corrector* fashion. From two successive points on the bifurcation curve,

$$P_1 = (c_1, a_1), \quad P_2 = (c_2, a_2),$$

i.e. two solutions of (50), we compute the direction vector

$$\mathbf{d} = (c_2 - c_1, a_2 - a_1) = (d^c, d^a). \tag{51}$$

We proceed to an initial guess P_3 for the next solution by moving a small increment s from P_2 in the direction $\mathbf{d}$:

$$P_3 = P_2 + s \cdot \mathbf{d} = (c_2 + s \cdot d^c, a_2 + s \cdot d^a). \tag{52}$$

This is the prediction step. Further, we require the solution P_* to lay on the line orthogonal to the one spanned by $\mathbf{d}$:

$$P_* = P_3 + \theta \cdot \mathbf{d}_\perp = \left(c_3 + \theta \cdot d^c_\perp, a_3 + \theta \cdot d^a_\perp\right), \quad d^c_\perp = -d^a, \quad d^a_\perp = d^c. \tag{53}$$

Note that the collocation algorithm described above is not optimal from the point of view of computational complexity. Indeed, one may use a pseudo-spectral algorithm in order to speed up the computations. A number of examples pertaining to similar equations and also more complex situations may be found in [22].

Table 2
Errors for the KdV equation.

Grid size	$\log_{10}(\|\|u_{\text{exact}} - u\|\|)_{L^2}$	$\log_{10}(\|\|u_{\text{exact}} - u\|\|)_{L^\infty}$	Ratio of successive L^2 errors
32	−2.30473	−1.55271	
64	−3.39842	−2.50547	12.407
128	−6.98265	−6.06670	3839.085

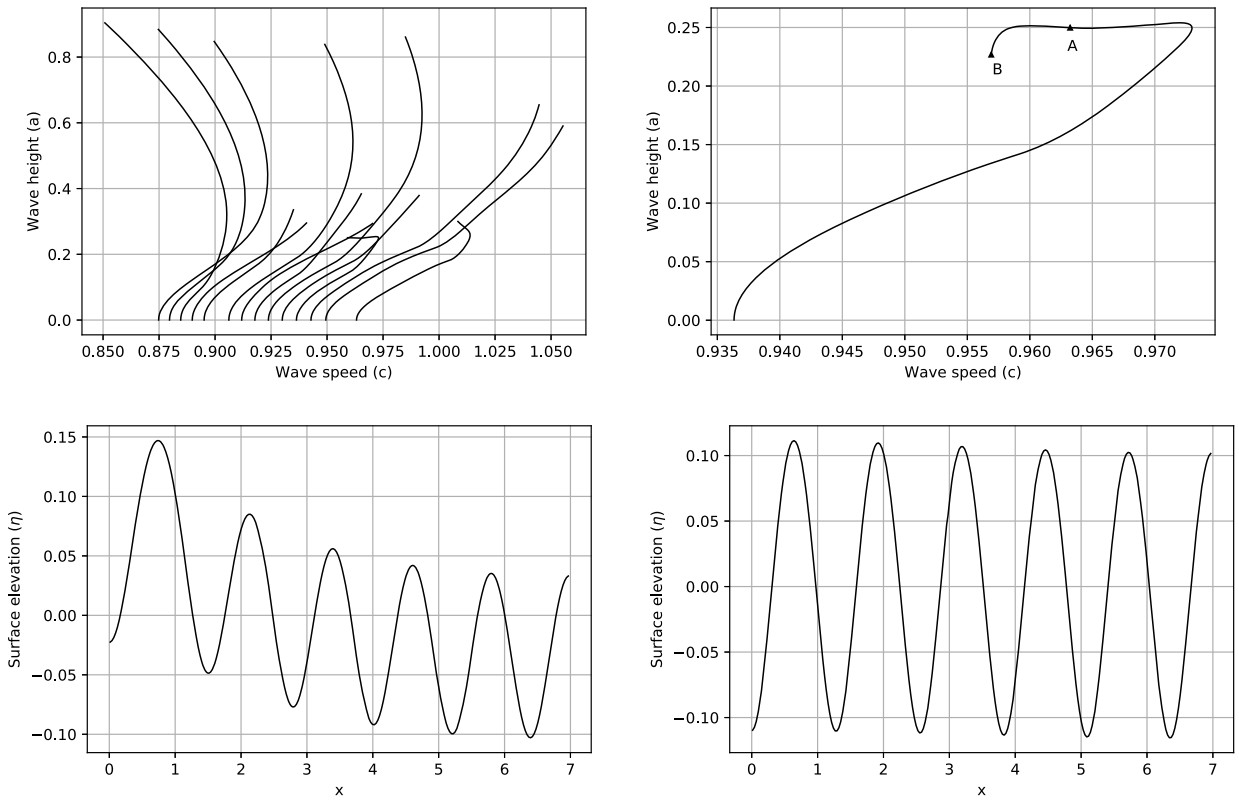

Fig. 4. Bifurcation branches and selected solution profiles for the case $U = c_0 v_0 + 0.1$, with wave numbers running from 0.05 to 1.00. Upper left panel shows a variety of branches. Upper right panel shows a close-up on one of the turning branches. Point A on the branch has approximate coordinates (0.963, 0.250), and B has approximate coordinates (0.957, 0.227). The lower left panel shows the solution profile at the point A. The lower right panel shows the solution profile at the point B.

6. Numerical results

In the special case when $U = c_0 v_0$, our derived model equation (32) reduces to the KdV-type equation

$$u_t + u_x + \frac{3}{2} u u_x - \gamma u_{xxx} = 0, \tag{54}$$

which is well-known for being an exactly integrable equation, with solitary wave solutions

$$u(x,t) = 2(c-1)\,\mathrm{sech}^2\left(\frac{1}{2}\sqrt{\frac{1-c}{\gamma}}(x - ct - x_0)\right). \tag{55}$$

Having an exact solution at our disposal, it is desirable to test the accuracy and implementation of the numerical routine. Table 1 summarizes our findings.

It can be seen the convergence is rather quick, in fact exponential, with increasing grid size. This is to be expected since exponential convergence of spectral schemes is a hallmark of solutions which have a domain of analyticity bounded away from the real axis [3]. In the case of nonzero capillarity, exact solutions are not available, and in our computations we aimed for a residual of equation (43) on the order of 10^{-8}, though smaller tolerances would also be possible.

We then did multiple runs to find steady solutions of equation (32) with different values of the shear velocity U, and with a wide range of admissible wavelengths L (corresponding for the most part to positive speed c). A plot like that in Fig. 3(a) was a typical result, showing three terminating and connecting bifurcation branches, and the wave profiles at

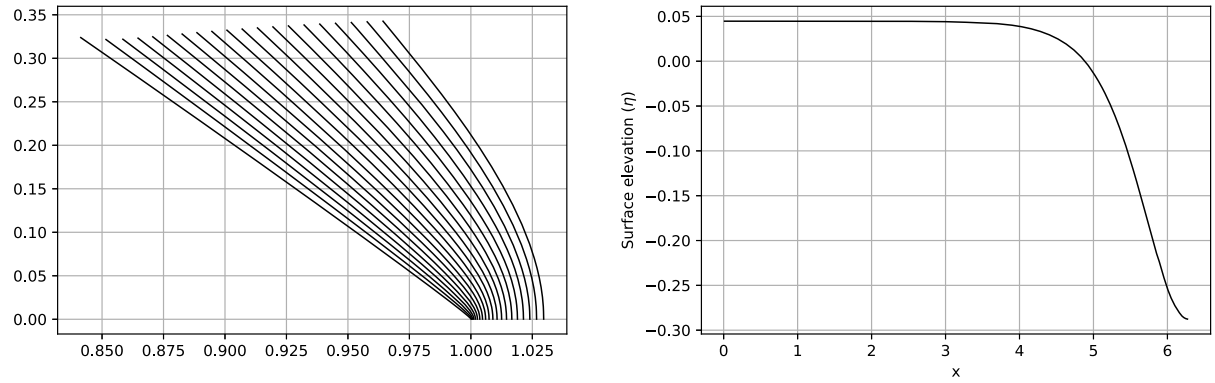

Fig. 5. Bifurcation branches and solution profiles for the KdV-type equation. No turning or terminating curves are present. The left panel shows typical bifurcation branch plots for the KdV case $U = c_0 v_0$, with wave numbers ranging from 0.05 to 1.00. The right panel shows a numerical KdV solution at the end of the branch corresponding to $k = 0.5$.

the points of connection. Note that the bifurcation points are obtained from the usual linear phase speed $c = \alpha(\xi)$, where $\xi = 2\pi/L$ is the wave number, and $\alpha(\xi)$ is given by (37). As can be seen in Fig. 3, for pairs of wavenumbers k and k^* which are multiples of one another, the bifurcation branches first cross without connecting, and then connect giving evidence to secondary bifurcations. The branches emanating from the wavenumbers k are gravity branches, which do not show signs of termination, though it should be noted that large-amplitude solutions are not physical. In contrast, the branches emanating from k^* are capillary-gravity branches, which show completely different behavior. These branches feature multiple turning points and eventually terminate by connecting to a pure gravity branch of the requisite wavenumber. Similar bifurcation patterns were found in [19]. Note that manual intervention was necessary if the bifurcation was to be continued beyond such a secondary bifurcation. The KdV case $U = c_0 v_0$ did not display such behavior, but values close to the critical value of $c_0 v_0$ did show terminating branches and secondary bifurcations.

It was then natural to pose the question of whether this is unique behavior for the KdV-type equation, i.e. that the non-termination of branches is a closed condition to the KdV case. Investigating this issue further, our numerical findings point to a conclusion of a closed condition, as secondary bifurcations appear as soon as the nonlocal operator has a non-zero coefficient. For example, Fig. 4 shows the case $U = c_0 v_0 + 0.1$, and it is clear that secondary bifurcations occur. The lower right panel of Fig. 4 shows the solution profile at point B, which clearly connects to a branch of smaller fundamental wavelength.

While the secondary bifurcations always happen for large-amplitude solutions, this phenomenon is probably connected with the fact that for all values of U except $U = c_0 v_0$, the dispersion curve is non-monotone. However, the precise manner in which this property of the linearized equation manifests itself far up in the strongly nonlinear regime in the bifurcation branch is not yet fully understood. (See Fig. 5.)

Another open problem is whether or not these bifurcation curves have an impact on the dynamic stability of these profiles. This issue is of major importance to the original question of whether large underwater lakes can stabilized by the hydrate layer, and at what depth one may consider underwater storage of CO_2 safe. The stability of the profiles obtained here will be the subject of future investigations.

Acknowledgements

The authors would like to thank Guttorm Alendal for bringing this problem to their attention. This research was supported by the European Commission grant no. 511176-2, the Research Council of Norway grant no. 239033/F2 and the Simons Foundation. The second author would like to thank the Isaac Newton Institute at Cambridge University where he was visiting during the preparation of this manuscript.

References

[1] T.B. Benjamin, Internal waves of permanent form in fluids of great depth, J. Fluid Mech. 29 (1967) 559–592.
[2] T.B. Benjamin, A new kind of solitary wave, J. Fluid Mech. 245 (1992) 401–411.
[3] M. Bjørkavåg, H. Kalisch, Exponential convergence of a spectral projection of the KdV equation, Phys. Lett. A 365 (4) (2007) 278–283.
[4] H. Borluk, H. Kalisch, Particle dynamics in the KdV approximation, Wave Motion 49 (2012) 691–709.
[5] P.G. Brewer, E.T. Peltzer, P. Walz, I. Aya, K. Yamane, R. Kojima, Y. Nakajima, N. Nakayama, P. Haugan, T. Johannessen, Deep ocean experiments with fossil fuel carbon dioxide: creation and sensing of a controlled plume at 4 km depth, J. Mar. Res. 63 (2005) 9–33.
[6] V.A. Dougalis, A. Duran, D. Mitsotakis, Numerical solution of the Benjamin equation, Wave Motion 52 (2015) 194–215.
[7] V.A. Dougalis, A. Duran, D. Mitsotakis, Numerical approximation of solitary waves of the Benjamin equation, Math. Comput. Simul. 127 (2016) 56–79.
[8] P.G. Drazin, W.H. Reid, Hydrodynamic Stability, 2nd edition, Cambridge University Press, 2004.
[9] M. Ehrnström, H. Kalisch, Global bifurcation for the Whitham equation, Math. Model. Nat. Phenom. 8 (2013) 13–30.
[10] I. Fer, P. Haugan, Dissolution from a liquid CO_2 lake disposed in the deep ocean, Limnol. Oceanogr. 48 (2003) 872–883.

[11] J. Hove, P.M. Haugan, Dynamics of a CO_2-seawater interface in the deep ocean, J. Mar. Res. 63 (2005) 563–577.
[12] H. Kalisch, Derivation and comparison of model equations for interfacial capillary-gravity waves in deep water, Math. Comput. Simul. 74 (2007) 168–178.
[13] H. Kalisch, J. Bona, Models for internal waves in deep water, Discrete Contin. Dyn. Syst. 6 (2000) 1–20.
[14] H. Kalisch, D. Moldabayev, O. Verdier, A numerical study of nonlinear dispersive wave models with SpecTraVVave, Electron. J. Differ. Equ. 2017 (62) (2017) 1–23.
[15] Y. Kobayashi, Physical behavior of liquid CO_2 in the ocean, in: Direct Ocean Disposal of Carbon Dioxide, 1995, pp. 165–181.
[16] P.K. Kundu, I.M. Cohen, Fluid Mechanics, Academic Press, 2008.
[17] D. Moldabayev, O. Verdier, H. Kalisch, SpecTraVVave, http://github.com/olivierverdier/SpecTraVVave, November 2016.
[18] K. Nealson, Lakes of liquid CO_2 in the deep sea, Proc. Natl. Acad. Sci. USA 103 (2006) 13903–13904.
[19] F. Remonato, H. Kalisch, Numerical bifurcation for the capillary Whitham equation, Physica D 343 (2017) 51–62.
[20] G.B. Whitham, Linear and Nonlinear Waves, Wiley, 1999.
[21] K. Yamane, I. Aya, S. Namie, H. Nariai, Strength of CO_2 hydrate membrane in sea water at 40 MPa, Ann. N.Y. Acad. Sci. 912 (2000) 254–260.
[22] J. Yang, Nonlinear Waves in Integrable and Nonintegrable Systems, vol. 16, SIAM, 2010.